Simulated optical imaging of orientation preference in a model of V1

Conference Paper · April 2003

DOI: 10.1109/CNE.2003.1196872 · Source: IEEE Xplore

2 authors, including:

Paul Sajda
Columbia University

195 PUBLICATIONS **3,752** CITATIONS

SEE PROFILE

Simulated Optical Imaging of Orientation Preference in a Model of V1

Jim Wielaard and Paul Sajda
Department of Biomedical Engineering, Columbia University, NY, USA

***Abstract*— Optical imaging studies have played an important role in mapping the orientation selectivity and ocular dominance of neurons across an extended area of primary visual cortex (V1). Such studies have produced images with a more or less smooth and regular spatial distribution of relevant neuronal response properties. This is in spite of the fact that results from electrophysiological recordings, though limited in their number and spatial distribution, show significant scatter/variability in the relevant response properties of nearby neurons. In this paper we present a simulation of the optical imaging experiments of ocular dominance and orientation selectivity using a computational model of the primary visual cortex. The simulations assume that the optical imaging signal is proportional to the averaged response of neighboring neurons. The model faithfully reproduces ocular dominance columns and orientation pinwheels in the presence of realistic scatter of single cell preferred responses. In addition,we find the simulated optical imaging of orientation pinwheels to be remarkably robust, with the pinwheel structure maintained up to an addition of ± 60 degrees of random scatter in the orientation preference of single cells. Our results suggest that an optical imaging result does not necessarily, by itself, provide any obvious upperbound for the scatter of the underlying neuronal response properties on local scales.**

***Keywords*— visual cortex, orientation hypercolumn, orientation pinwheel, optical imaging, ocular dominance column**

I. Introduction

The very first stage of cortical processing of visual information in mammals takes place in area V1, primary visual cortex. Single cells in V1 show a wide range of response properties. When comparing neighboring cells, any one of these response properties can demonstrate significant variance/scatter [1]. Despite this fact, optical imaging experiments show a remarkably organized spatial distribution over V1 for some of these response properties. In particular, optical imaging in cat and monkey show that the spatial arrangement of the maximum response to edges (or bars) of a given angle, varies smoothly across preferred orientation. These results also show that the preferred orientation map predominately forms "pinwheels" [2], [3], [4]. In the same experiments, electrode measurements of maximal responses of neighboring cells show a scatter on the order of $\pm 15 \sim 20$ degrees in visual angle space, corresponding to 30-50% the size of the observed orientation pinwheels in the cortex [5].

The question arises, given such a large scatter in the responses of single neurons, to what extent does the optical imaging signal itself, and the methods used to compute the preferred response, contribute to the observation of a smooth distribution of orientation domains and pinwheels in V1. This question is difficult to address in a strictly experimental setting. For example it is extremely challenging, if not impossible with current measurement techniques, to obtain single cell responses for a reasonably large number of neighboring cells. However such single cell responses are necessary so that their combined response can be related to the optical imaging signal and resultant maps.

In this paper we report on these issues within the framework of a computational model we have developed of multiple orientation hypercolumns of V1. We first begin by providing a concise description of the model, followed by the methods used to simulate the optical image. We then present results showing that spatial averaging plays an important role in determining the fidelity of the recovered maps. Such averaging can be a result of the imaging process, or the method for computing the preferred orientation, given the measured optical signal.

II. The Model

In this paper we provide only a brief description of our model of V1. Readers interested in a more detailed description and characterization are referred to [6], [7]. The model consists of a two dimensional layer of N conductance based integrate-and-fire point neurons (one compartment). Each neuron, indexed by i, is assigned a membrane potential $V_i(t)$ and a spike train $\mathcal{S}_i(t) = \sum_k \delta(t - t_{i,k})$, where t is time and $t_{i,k}$ is the kth spike of the ith neuron. Whenever the membrane potential reaches a threshold level, it is reset and a spike is registered. Each membrane potential obeys an equation of the form

$$\begin{aligned} C_i \frac{dV_i(t)}{dt} &= -\lambda_i(V_i(t) - V_L) \\ &\quad -g_{E,i}(t, [\mathcal{S}], \eta_E)(V_i(t) - V_E) \\ &\quad -g_{I,i}(t, [\mathcal{S}], \eta_I)(V_i(t) - V_I) + I_i^{ext}(t) \\ &\quad i = 1, \ldots, N \, . \end{aligned}$$

Where

$$g_{E,i}(t, [\mathcal{S}], \eta_E) = g_i^{LGN}(t) + \eta_{E,i}(t) + g_{E,i}^{cor}(t, [\mathcal{S}]) \, ,$$
$$g_{I,i}(t, [\mathcal{S}], \eta_I) = \eta_{I,i}(t) + g_{I,i}^{cor}(t, [\mathcal{S}]) \, ,$$

Here, C_i is the membrane capacitance, V_L, V_E and V_I are the reversal potentials of leakage, excitation and inhibition respectively, λ_i, $g_{E,i}$ and $g_{I,i}$ are the leakage, excitatory and inhibitory conductances impinging on neuron i. The quantities η_E and η_I are external stochastic terms, $I_i^{ext}(t)$ is an external current and $[\mathcal{S}]$ is shorthand notation for $\mathcal{S}_1(t), \mathcal{S}_2(t), \ldots, \mathcal{S}_N(t)$ to indicate that neuron i is coupled in principle to all excitatory and inhibitory neurons in the system. Area V1 receives the majority of its direct visual

input via the lateral geniculate nucleus (LGN). LGN axons terminate predominantly on simple cells in the input layers 4C and are purely excitatory. Therefore, in the model, their contribution enters into the excitatory conductance of the simple cells, the terms $g^{cor}_{\cdot,i}(t,[\mathcal{S}])$ are the contributions from the cortical excitatory and inhibitory neurons,

$$g^{cor}_{\cdot,i}(t,[\mathcal{S}]) = \int_{-\infty}^{+\infty} ds \sum_{j\in\mathcal{P}(\cdot)} \mathcal{C}_{i,j}(||\vec{x}_i - \vec{x}_j||) G_{\cdot,j}(t-s)\mathcal{S}_j(s) \; .$$

The LGN neurons are modelled as rectified center surround linear spatiotemporal filters, N_0 of them feeding into a cortical simple cell,

$$g^{LGN}_j(t) = \sum_{i=1}^{N_0} \left\{ g^0_j + \int_0^t ds \int d^2x G^{LGN}(t-s) A(\vec{x}_j{}^i - \vec{x}) I(\vec{x},s) \right\}^+ ,$$

where $I(\vec{x},s)$ is the stimulus and $\vec{x}_j{}^i$ is the receptive field center of the ith LGN cell feeding into the jth cortical (simple) cell.

For simulations, these equations are numerically integrated using a second order Runge Kutta method with a $\Delta t = 0.1$ ms. Neuronal responses are time averaged over 4 s periods.

Ocular dominance and the pinwheel structure of preferred orientation responses to bars or edges is present in the model at the level of the LGN input. No scatter is introduced in ocular dominance at the level of the LGN input; all scatter we observe in this property in the simulations is a consequence of the cortical interactions in the model. The scatter introduced at the level of the LGN in the orientation preference of the LGN input in simple cells together with a significant contribution of the cortical interactions the model, produces realistic scatter in these properties over the total (simple and complex) population of cells, as we will show below. All parameters, such as neuron density, fraction of inhibitory and excitatory cells, fraction of simple and complex cells, axon and dentritic sizes, synaptic and LGN time scales are set to the experimentally derived values know for the magno input layer $4C\alpha$ of the macaque monkey (see references in [6], [7]).

III. Simulated Optical Imaging Results

In our model, we measure single cell responses (membrane potential and spike train) to drifting grating stimuli of fixed spatial and temporal frequency and contrast, for multiple orientations and directions $\theta_k = 2k\pi/K$, $k = 0,\ldots,K-1$. These stimuli are independently presented to the left and right eye.

In order to make the connection between the optical imaging experiments performed in vivo, we assume that, to a first order approximation, the *raw* optical imaging signal $r^{\rm opt}_i(\theta_k)$ is related to the single cell responses $r_i(\theta_k)$ (membrane potential or firing rate), via the relation

$$r^{\rm opt}_i(\theta_k;n) \propto \frac{1}{n} \sum_{j\in\mathcal{N}_n(i)} r_j(\theta_k) \; ,$$

where $\mathcal{N}_n(i)$ is a neighborhood of n cells of neuron i. Using this equation we can produce an arbitrary "optical" imaging result for our model by further processing of $r^{\rm opt}_i(\theta_k;n)$ in the same spirit as is done in the *in vivo* optical imaging experiment we are trying to model [3], [4].

We compute ocular dominance $\mathcal{O}_i(n)$ for a given pixel of our model cortex given the simulated optical signals for left eye (L) and right eye (R),

$$\mathcal{O}_i(n) = \begin{cases} \text{L} & \text{if } \sum_k r^{\rm opt}_{i,L}(\theta_k;n) \geq \sum_k r^{\rm opt}_{i,R}(\theta_k;n) \\ \text{R} & \text{if } \sum_k r^{\rm opt}_{i,L}(\theta_k;n) < \sum_k r^{\rm opt}_{i,R}(\theta_k;n) \end{cases} .$$

The result for a model configuration with 16 orientation hypercolumns (4-by-4) is shown in Figure 1. The raw data (one neuron per pixel) are shown in the left panel, and responses averaged over the twelve nearest neighbors are shown in the right panel. Averaging makes the ocular dominance bands clearly visible. The distortion we observe with respect to ideal vertical bands is strictly a result of the cortical interactions.

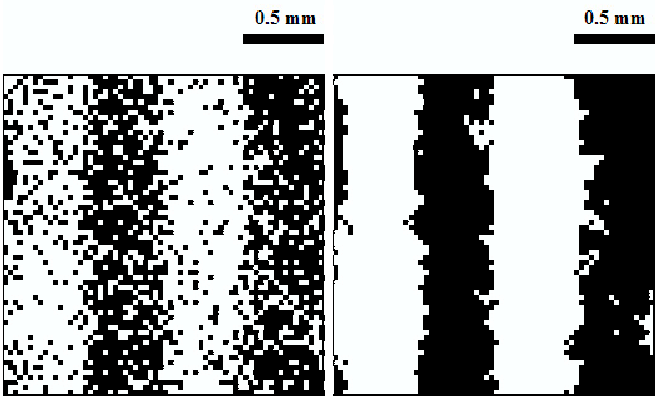

Fig. 1. Ocular dominance bands obtained in a 4-by-4 orientation hypercolumn configuration of the model. Left panel: raw data, one neuron per pixel. Right panel: results when responses are averaged over 12 nearest neighbors.

With regard to imaging the spatial organization of orientation preference $\Theta_i(n)$ we used two methods. First, we simply use the angle of maximum response as our imaging variable,

$$\Theta^M_i(n) = \max_{\theta_k} \left\{ r^{\rm opt}_{i,L}(\theta_k;n) + r^{\rm opt}_{i,R}(\theta_k;n) \right\}, \quad \mod(\pi).$$

Second, we use a "averaged difference vector" response which is frequently used in optical imaging experiments,

$$\Theta^V_i(n) = \frac{1}{2} \arg \sum_k \left\{ r^{\rm opt}_{i,L}(\theta_k;n) + r^{\rm opt}_{i,R}(\theta_k;n) \right\} e^{2i\theta_k}.$$

As in real cortex, single cell preferred orientation responses in our model display large spatial scatter. For the case of orientation preference, this scatter can be characterized by

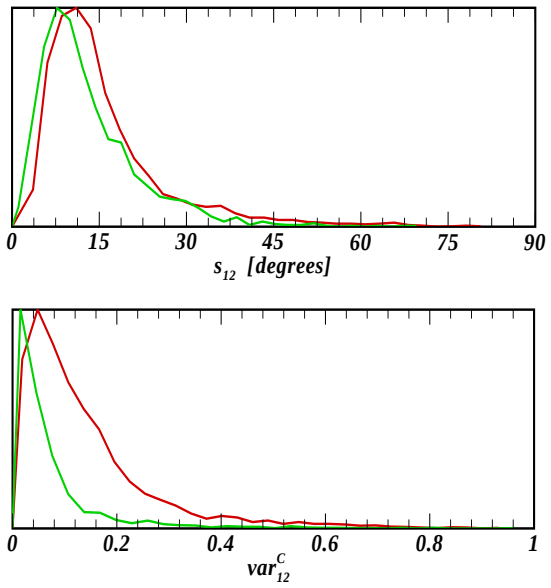

Fig. 2. Probability distribution functions of the averaged scatter $s_{12}(\Theta^V_i(1)$ and circular variance $\text{var}^C_{12}(\Theta^V_i(1)$ for $n = 12$ nearest neighbors and the "raw" data ($n = 1$) obtained from "average difference vector" method. Shown are the scatter in the LGN input in simple cells (green) and the scatter in the cortex (all cells) (red). The difference bewteen the two curves is a result of the cortical interactions.

the mean value of the circular variance (CV) of the imaging variable,

$$\text{var}^C_n(\Theta^{\cdot}_i(m)) = 1 - \frac{1}{n}\left|\sum_{j\in\mathcal{N}_n(i)} e^{2i\Theta^{\cdot}_j(m)}\right| ,$$

or, the average scatter, keeping in mind responses are periodic with period π,

$$\text{s}_n(\Theta^{\cdot}_i(m)) =$$

$$\frac{1}{n}\sum_{j\in\mathcal{N}_n(i)} \min\left[\left|\Theta^{\cdot}_j(m) - \Theta^{\cdot}_i(m)\right|,\right.$$

$$\left.\left|\Theta^{\cdot}_i(m) + \pi - \Theta^{\cdot}_j(m)\right|\right] .$$

Results are shown in figures 2 to 5. From the probability distribution functions in figure 2 we see that the scatter in orientation preference in the model is increased by the cortical interactions (green vs. red curves in figure 2). It is on the average about $\pm 15 \sim 20$ degrees, which agrees well with what is observed experimentally [2]. Raw data results (single cell responses with $n = 1$) for both methods are shown in Figure 3. Both methods generate pinwheels, with the vector average method having a smaller mean CV except perhaps at the pinwheel centers. Results after averaging the responses over 12 nearest neighbours (simulating additional optical blurring) are shown in figure 4. Both methods yield pinwheel structure. Figure 5 demonstrates the breakdown of the pinwheel structure. The stucture is maintained even after adding an additional ± 45 degrees random scatter in orientation preference of single cells. Not until scatter reaches ± 60 degrees over that observed *in vivo* does the pinwheel structure begin to degrade. Thus the orientation map generated via optical imaging can hide the underlying variablity in the preferred neural responses, even for scatter magnitudes which result in shifts that produce local distributions of single cells with orthongonal preferred orientations.

IV. Conclusion

In this paper we have presented simulation results of optical imaging experiments of V1 using using a computational model of the primary visual cortex. We find that the model can reproduce the ocular dominance and orientation pinwheel strcuture, observed *in vivo*, in the presence of physiologically realistic spatial variablity/scatter of single cell preferred response. In addition, we use the model to demonstrate that the orientation pinwheel structure observed via the simulated optical imaging is extremely robust to spatial scatter in the preferred angle, with the stucture maintained up to ± 60 degrees of additional random scatter in orientation preference. Thus, the model would predict that maps created via optical imaging of real cortex provide little insight into the underlying scatter of individual neuronal preferred response properties, in particular on scales sufficiently local with respect to the resolution used in the imaging.

Acknowledgments

This work was supported by the DoD Multidisciplinary University Research Initiative (MURI) program administered by the Office of Naval Research under Grant N00014-01-1-0625 as well as a grant from the National Imagery and Mapping Agency, NMA201-02-C0012. We thank Xiaowei Liu for assistance in the optical imaging simulations.

References

[1] G. DeAngelis, R. Ghoose, I. Ohzawa, and R. Freeman, "Functional micro-organization of primary visual cortex: receptive field analysis of nearby neurons," *J Neuroscience*, vol. 19, pp. 4046–4064, 1999.

[2] T. Bonhoeffer and A. Grinvald, "Iso orientation domains in cat visual cortex are aranged in pinwheel like patterns," *Nature*, vol. 353, pp. 429–431, 1991.

[3] G. Blasdel, "Differential imaging of ocular dominance and orientation selectivity in monkey striate cortex," *J Neuroscience*, vol. 12, pp. 3115–3138, 1992.

[4] ——, "Orientation selectivity, preference, and continuity in the monkey striate cortex," *J Neuroscience*, vol. 12, pp. 3139–3161, 1992.

[5] P. Maldonado, I. Godecke, C. Gray, and T. Bonhoeffer, "Orientation selectivity in pinwheel centers in cat striate cortex," *Science*, vol. 276, pp. 1551–1555, 1997.

[6] D. McLaughlin, R. Shapley, M. Shelley, and J. Wielaard, "A neuronal network model of macaque primary visual cortex (V1); orientation selectivity and dynamics in the input layer $4c\alpha$," *Proc Natl Acad Sci USA*, vol. 97, pp. 8087–8092, 2000.

[7] J. Wielaard, M. S. andD. McLaughlin, and R. Shapley, "How simple cells are made in a nonlinear network model of the visual cortex," *J Neuroscience*, vol. 21, pp. 5203–5211, 2001.

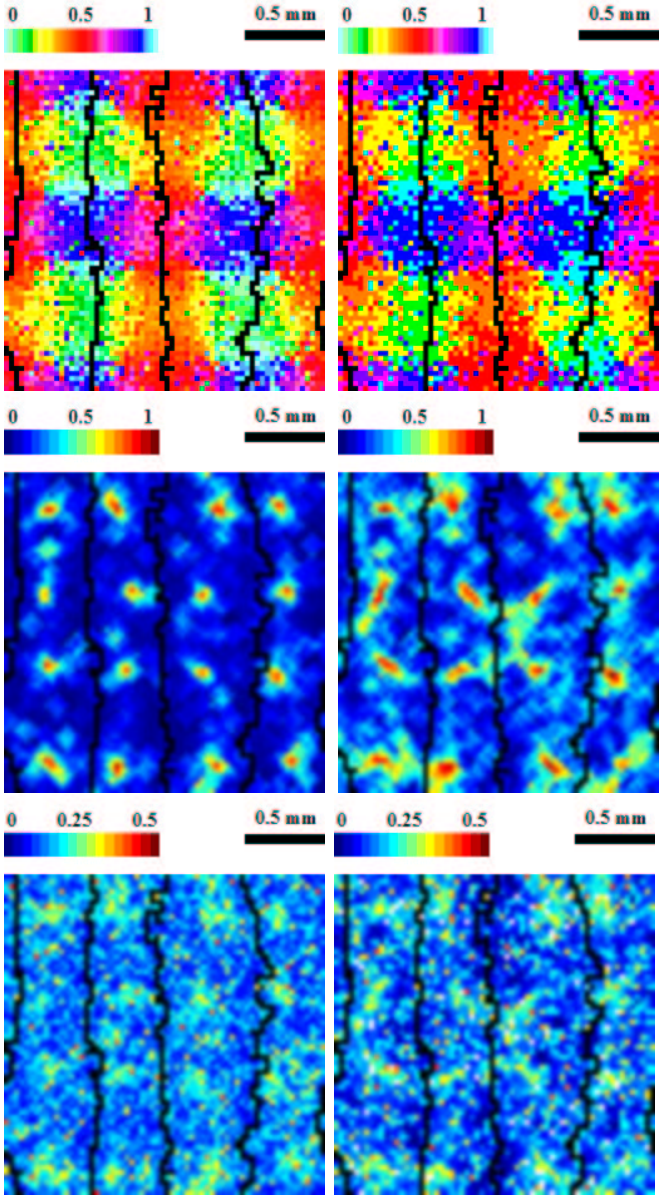

Fig. 3. Preferred angle $\Theta_i^V(1)$ as obtained from "averaged difference vector method" (left column) and $\Theta_i^M(1)$ as obtained from the maximum response method (right column). The dark lines are the borders between ocular dominance columns shown in figure 1. Top panels are the spatial distribution of the preferred angle for $n = 1$ (raw data) over the 16 orientation hypercolumns. Middle panels are the circular variance of the preferred angle calculated over 12 nearest neighbors $\mathrm{var}_{12}^C(\Theta_i^:(1))$, lower panel the average scatter $\mathrm{s}_{12}(\Theta_i^:(1))$ again calculated over 12 nearest neighbors. All angles are normalized to π.

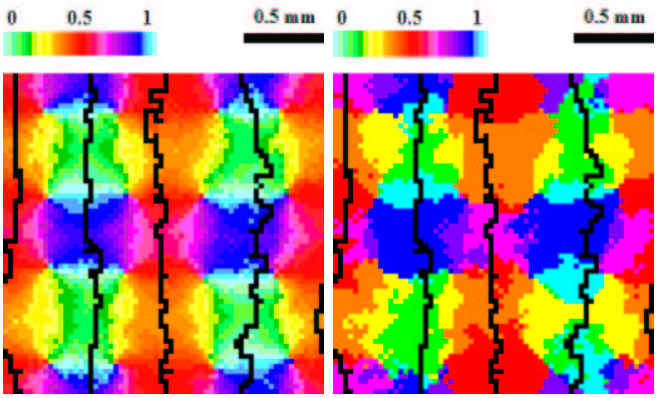

Fig. 4. Preferred angle $\Theta_i^V(n)$ as obtained from "average difference vector" method (left), and $\Theta_i^M(n)$ as obtained from the maximum response method (right). The dark lines are the borders between ocular dominance columns shown in figure 1. Averages are computed over $n = 12$ nearest neighbors. Angles are normalized to π.

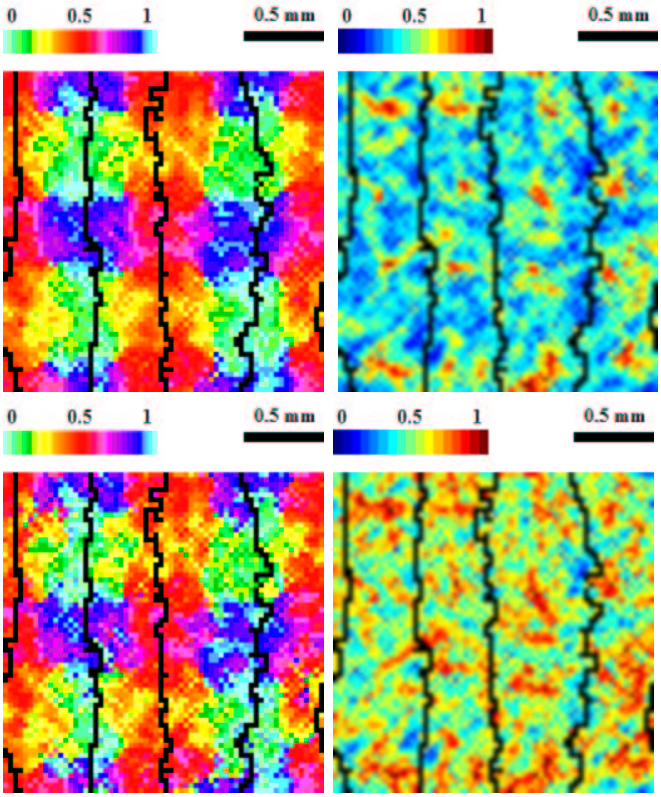

Fig. 5. Spatial organization of the preferred angle $\Theta_i^V(n)$ of responses averaged over $n = 12$ nearest neighbours (left column) when ± 45 degrees random scatter is added (top) in single cell responses, and with ± 60 degrees random scatter added (bottom). The right column shows the corresponding circular variance. The breakdown of the pinwheel structure at ± 60 degrees added random scatter is clear.